View metadata, citation and similar papers at core.ac.uk

brought to you by CORE

provided by MDC Repository

OPEN ACCESS

Repository of the Max Delbrück Center for Molecular Medicine (MDC) Berlin (Germany)
http://edoc.mdc-berlin.de/13953/

Detailing the relation between renal T2* and renal tissue pO2 using an integrated approach of parametric magnetic resonance imaging and invasive physiological measurements

Pohlmann, A., Arakelyan, K., Hentschel, J., Cantow, K., Flemming, B., Ladwig, M., Waiczies, S., Seeliger, E., Niendorf, T.

Published in final edited form in :
Investigative Radiology. 2014 Aug ; 49 (8) : 547-560 | doi: 10.1097/RLI.0000000000000054
Lippincott Williams & Wilkins (U.S.A.) ►

Detailing the relation between renal T_2* and renal tissue pO_2 using an integrated approach of parametric magnetic resonance imaging and invasive physiological measurements (MR-PHYSIOL)

Andreas Pohlmann, PhD,[1]* Karen Arakelyan, MD,[1,2]* Jan Hentschel,[1] Kathleen Cantow, DVM,[2] Bert Flemming, MD,[2] Mechthild Ladwig, DVM,[2] Sonia Waiczies, Dr. rer.med.,[1] Erdmann Seeliger, DM,[2]* and Thoralf Niendorf, PhD[1]*§

* These authors contributed equally to this work.

[1] Berlin Ultrahigh Field Facility (B.U.F.F.), Max Delbrück Center for Molecular Medicine, Berlin, Germany

[2] Institute of Physiology, Charité – Universitätsmedizin Berlin, Campus Mitte, and Center for Cardiovascular Research, Berlin, Germany

§ Corresponding Author:

Prof. Dr. Thoralf Niendorf
Berlin Ultrahigh Field Facility (B.U.F.F.)
Max Delbrück Center for Molecular Medicine
Robert Rössle Str. 10
13125 Berlin, Germany
Tel: +49 30 9406 4505
Fax: +49 30 9406 49176
Email: thoraf.niendorf@mdc-berlin.de

Short title: Detailing renal T_2*/pO_2 relation by MR-PHYSIOL

Keywords: magnetic resonance imaging, BOLD, acute kidney injury, integrative physiology, MR-PHYSIOL, renal oxygenation, renal perfusion

Acknowledgement

This work was funded by a grant from the German Research Foundation (NI 532/9-1, FOR 1368). We wish to acknowledge Ariane Anger for expert technical assistance.

Abstract

Objectives: This study is designed to detail the relation between renal T_2* and renal tissue pO_2 using an integrated approach that combines parametric MRI and quantitative physiological measurements (MR-PHYSIOL).

Materials and Methods: Experiments were performed in 21 male Wistar rats. *In vivo* modulation of renal hemodynamics and oxygenation was achieved by brief periods of aortic occlusion, hypoxia and hyperoxia. Renal perfusion pressure (RPP), renal blood flow (RBF), local cortical and medullary tissue pO_2 and blood flux were simultaneously recorded together with T_2*, T_2 mapping and MR based kidney size measurements (MR-PHYSIOL). MRI was carried out on a 9.4 Tesla small animal MR system. Relative changes in the invasive quantitative parameters were correlated with relative changes in the parameters derived from MRI using Spearman's analysis and Pearson's analysis.

Results: Changes in T_2* qualitatively reflected tissue pO_2 changes induced by the interventions. T_2* versus pO_2 Spearman rank correlations were significant for all interventions, yet quantitative translation of T_2*/pO_2 correlations obtained for one intervention to another intervention proved not appropriate. The closest T_2*/pO_2 correlation was found for hypoxia & recovery. The inter-layer comparison revealed closest T_2*/pO_2 correlations for the outer medulla and showed that extrapolation of results obtained for one renal layer to other renal layers must be made with due caution. For T_2* to RBF relation significant Spearman correlations were deduced for all renal layers and for all interventions. T_2*/RBF correlations for cortex and outer medulla were even superior to those between T_2* and tissue pO_2. The closest T_2*/RBF correlation occurred during hypoxia & recovery. Close correlations were observed between T_2* and kidney size during hypoxia & recovery and for occlusion & recovery. In both cases, kidney size correlated well with renal vascular conductance, as did renal vascular conductance with T_2*. Our findings indicate that changes in T_2* qualitatively mirror changes in renal tissue pO_2 but are also associated with confounding factors including vascular volume fraction and tubular volume fraction.

Conclusions: Our results demonstrate that MR-PHYSIOL is instrumental to detail the link between renal tissue pO_2 and T_2* *in vivo*. Unravelling the link between regional renal T_2* and tissue pO_2 - including the role of the T_2* confounding parameters vascular and tubular volume fraction and oxyHb dissociation curve - requires further research. These explorations are essential before the quantitative capabilities of parametric MRI can be translated from

experimental research to improved clinical understanding of hemodynamics/oxygenation in kidney disorders.

Keywords: magnetic resonance imaging, BOLD, quantitative MRI, acute kidney injury, integrative physiology, MR-PHYSIOL, renal oxygenation, renal perfusion

Introduction

Renal tissue hypoperfusion and hypoxia are considered to be pivotal links in the pathophysiological chain of events that leads to acute kidney injury (AKI) as well as the one that promotes progression from AKI to chronic kidney diseases (CKD) [1-7]. Imbalance between renal oxygen supply and demand also appears to play a prominent role in the pathophysiology of diabetic nephropathy [8, 9]. Making ultimate statements on the role of renal hypoperfusion and hypoxia for these renal disorders is elusive since *in vivo* assessment of renal hemodynamics and oxygenation constitutes a challenge. All modalities available in today's experimental and translational research practice have inherent shortcomings and methodological constraints [2, 10-12].

Obtaining insights into renal perfusion and oxygenation under (patho)physiological conditions by means of non-invasive diagnostic imaging is conceptually appealing. Blood oxygen level dependent (BOLD) magnetic resonance imaging (MRI) and quantitative parametric mapping of the MR relaxation times T_2* and T_2 are thought to provide surrogates of renal tissue oxygenation in preclinical and clinical studies [10, 12-35]. This assumption is based upon the T_2*/T_2 dependence on O_2-saturation of hemoglobin (Hb) and motivated by the link between O_2-saturation of Hb, blood partial pressure of O_2 (pO_2) and tissue pO_2. Although T_2* and T_2 basically reflect the amount of deoxyHb while pO_2 represents the concentration of oxygen, changes in renal T_2*/T_2 and tissue pO_2 may be closely related. Yet their link is also known to be sensitive to the oxyHb dissociation curve, haematocrit, and to the vascular volume fraction [2, 11, 36-38]. This added complexity confounds interpretation of BOLD weighted MRI and parametric T_2* mapping data obtained from patients with AKI and CKD [11, 39-41]. For an unambiguous physiological interpretation of renal T_2* a calibration with quantitative physiological measurements including renal tissue pO_2 is required. For this purpose an integrative multi-modality approach is essential - as underlined in a recent call for further explorations into hemodynamic influences on kidney oxygenation [4] - before the capabilities of parametric MRI can be translated from experimental research to an improved clinical understanding of hemodynamics/oxygenation in AKI and CKD.

An integrated approach that combines parametric MRI with quantitative physiological measurements is prudent to detail the link between renal T_2* and renal tissue oxygenation. Quantitative characterization of renal hemodynamics and oxygenation comprises very well

established invasive methods that assess perfusion of the entire kidney, regional perfusion and regional oxygenation in the intact animal [2, 12, 42]. MRI offers full kidney coverage, (sub)millimeter spatial resolution, (sub)minute temporal resolution and support of longitudinal studies [10, 12-18, 39, 43]. The validity and efficacy of parametric MRI for quantitative and spatiotemporal characterization of renal tissue perfusion and oxygenation under different functional conditions has not been systematically examined yet and remains to be established. A very limited number of studies attempted to draw a link between established invasive methods and T_2*-weighted MRI [44-46]. These studies relied on either comparing MRI and invasive physiological measurements performed in independent cohorts of animals [45, 46] or on T_2* and pO_2 recorded in the same animal but at different times [33] or in different kidneys (contralateral vs. ipsilatereal) [47].

Realizing the challenges and opportunities of using an integrated multi-modality approach for detailing the relation between renal T_2*/T_2 and renal oxygenation we hypothesized that simultaneous tracking of invasive physiological parameters and MR parameters derived from the same kidney will elucidate to which extent alterations of physiological parameters are reflected by changes in renal T_2* and T_2. To test this hypothesis an integrative hybrid approach was employed that combines established invasive measurements including renal perfusion pressure, renal blood flow, local blood flux and tissue pO_2 with T_2*, T_2 mapping and MR based kidney size measurements (MR-PHYSIOL) [12]. *In vivo* modulation of renal hemodynamics and oxygenation was achieved by standardized (patho)physiologically relevant but reversible interventions, including brief periods of aortic occlusion, hypoxia and hyperoxia. Relative changes in the invasive quantitative parameters were correlated with relative changes in the parameters derived from MRI.

Materials and Methods

Animal Preparation

All investigations were approved by the Animal Welfare Department of [redacted] State Office of Health and Social Affairs in accordance with the [redacted] Animal Protection Law. The spatial constraints dictated by the MR environment required the use of relatively small rats. For this reason, experiments were performed in 21 male Wistar rats (aged 12-13 weeks, body mass (BM) 336±27 g; Harlan-Winkelmann, Borchen, Germany). The animals were allowed ad libitum food (standard diet) and water and were housed under standard conditions with environmental enrichment. For anesthesia urethane (20% in distilled water; 6 mL kg^{-1} BM i.p.; Sigma-Aldrich, Steinheim, Germany) was used throughout the surgical preparation and the MRI examination. This approach provides anesthesia for several hours and leaves cardiovascular reflexes largely undisturbed. Body temperature was maintained at 37 °C by means of a mat through which warm water circulates.

Monitoring of absolute arterial blood pressure that corresponds with renal perfusion pressure (RPP; in mm Hg) was achieved by placing a catheter into the femoral artery with its tip towards the aorta [12]. The catheter was connected to a pressure transducer (DT-XX, Viggo-Spectramed, Swindon, UK) and amplifier (TAM-A Plugsys Transducer; Hugo Sachs Elektronik – Harvard Apparatus GmbH, Mach-Hugstetten, Germany).

Absolute measurement of renal blood flow (RBF; in mL min^{-1}) used an ultra sound transit time flow probe (MC2PSB-MRI, Transonic Systems Inc., Ithaca, USA), equipped with a customized ceramic reflector, positioned around the left renal artery. Extra care was taken for the probe positioning [12] since pressure of the relatively large flow probe on the aorta, the renal artery and vein and/or the kidney itself bears the risk to cause ischemia or congestion of the kidney. In order to prevent these complications RBF values and the overall condition of the kidneys (e.g., surface coloring and its homogeneity) were carefully monitored during the entire preparation. After positioning of the animal in the MR scanner a low renal T_2* (in particular medullary T_2*) was used as an additional criterion for early detection of any flow probe-induced renal ischemia. In two cases the flow probe was alternatively placed around the renal vein. In three animals even this probe position was not feasible so that the probe was omitted entirely. To achieve appropriate coupling of the ultrasound flow probe to the tissue,

the abdominal cavity was filled with saline via a catheter (38°C; replenished throughout experiment).

Renal vascular conductance [ml min^{-1} $mmHg^{-1}$] (the inverse of resistance) was calculated by dividing RBF [ml min^{-1}] by RPP [mmHg]."

Measurement of absolute tissue pO_2 (in mm Hg) and erythrocyte flux (arbitrary units) was enabled by combined laser-Doppler-flux/pO_2 probes (pO_2 E-Series Sensor; Oxford Optronics, Oxford, UK) that were inserted into the renal tissue. One probe was placed in the medullary region, at 4-mm depth. Another probe was placed in the cortical region by advancing it from the caudal extremity, centrally through the kidney to the cortical layer of the cranial extremity [12].

For induction of aortic occlusion during the MR study a remotely operated inflatable cuff was positioned around the aorta right above the renal arteries [12]. Core body temperature was monitored by means of a fiber-optic temperature probe (T1S-02-B05, Neoptix, Quebec, Canada) placed in the rectum.

The flux/pO_2 probe extensions were passed through the abdominal wall using a small incision in the left inguinal region. All other cables together with the lines for the aortic cuff, for saline supply, cables of the perivascular flow probe and fiber-optic connection of the body temperature probe were passed through the caudal cutting edge of the median abdominal incision. The abdominal wall was closed by a continuous suture. For a more detailed description and discussion of the probe implantation and fixation please refer to [12].

MR Imaging and Parametric Mapping

MR imaging was carried out on a 9.4 Tesla small animal MR system (Bruker Biosec 94/20; Bruker Biospin, Ettlingen, Germany) equipped with a linear polarized birdcage volume resonator used for RF transmission in conjunction with a curved four channel receive surface RF coil array (Bruker Biospin, Ettlingen, Germany) customized for rats. T_2 weighted pilot scans for geometrical planning and slice positioning were acquired first. Local volume selective shimming of the magnetic field homogeneity on a voxel accommodating the kidney only was conducted using an automatic optimization algorithm based on FID length. To visualize the position of the pO_2 and Laser-flux probes 3D multi gradient echo (MGE) imaging of the entire kidney was performed (repetition time = 20 ms, echo time = 2.85 ms, total acquisition time = 2 min 55 s, field of view (FOV) = (38.2 x 48.5 x 21.9) mm^3, matrix

size = 126 x 120 x 72, spatial resolution = (303 x 404 x 304) μm^3). The same 3D image set was used for slice positioning applied in the parametric mapping protocols.

Interleaved T_2* and T_2 mapping were performed with respiratory gated (Model 1025, SA Instruments, New York, NY, USA) imaging protocols. For T_2* mapping a multi gradient echo (MGE) sequence (repetition time = 50 ms, number of echoes = 10, first echo time = 1.43 ms, echo time increment = 2.14 ms, averages = 4) with a total acquisition time of 1 min 20 s was used. T_2 mapping employed a multi-echo spin-echo (MSME) sequence (repetition time = 550 ms, number of echoes = 7, first echo time = 10 ms, echo spacing 10 ms, averages = 1), resulting in a total acquisition time of 1 min 40s. A coronal oblique slice was placed across the kidney so that the cortical and medullary pO_2 and Laser-flux probes were located within the imaging plane as illustrated in Figure 1. An in-plane spatial resolution of (226 x 445) μm^2 (FOV = (38.2 x 50.3) mm^2, matrix size = 169 x 113 zero-filled to 169 x 215) and a slice thickness of 1.4–1.5 mm were employed.

The presence/absence of blood flow in the major renal blood vessels was confirmed with time-of-flight (TOF) MR angiography (MRA) performed at baseline and immediately after onset of aortic occlusion and onset of reperfusion. For TOF-MRA a spoiled gradient echo technique (2D FLASH, TR = 11 ms, TE = 3 ms, flip angle = 80 degree) with a spatial in-plane resolution of (200 x 268) μm^2) and 15 slices (slice thickness = 1.0 mm) was applied.

Experimental Protocol and Standardized Reversible Interventions

Throughout the experiments the rats were continuously provided with air (or other gas mixtures) at a rate of 1000 mL min^{-1} provided by a respiratory mask placed around the muzzle of the spontaneously breathing rat. Following positioning of the rat in the isocenter of the MR scanner, scanner adjustments and slice positioning was conducted followed by baseline T_2* and T_2 mapping. Subsequently, short-term reversible interventions were performed: hyperoxia, aortic occlusion, and hypoxia, each followed by recovery.

Aortic occlusion was initiated by inflating the remotely controlled suprarenal aortic occluder and verified by absence of the flow-based blood signal in renal TOF-MRA. Occlusion lasted 3 minutes. One set of T_2*/T_2 maps was acquired before the occluder was deflated to re-establish renal blood flow. The recovery period comprised 9 minutes and three sets of T_2*/T_2 mapping.

Hypoxia was induced by decreasing the inspiration fraction of oxygen (FiO_2) to 8% via changing the gas flow through the respiratory mask to 8% O_2 / 92% N_2. FiO_2 was monitored

using a Capnomac AGM-103 (Datex GE, Chalfont St. Gils, UK). T_2*/T_2 mapping were performed twice during hypoxia. The first set was acquired immediately after onset of hypoxia, the second set was started 5 minutes after onset of hypoxia. Following hypoxia of approximately 12 minutes FiO_2 was restored to 21% (normoxia, room air). The recovery period of 15 minutes comprised four sets of T_2*/T_2 maps. Hyperoxia was induced using the same protocol, with the exception that FiO_2 was increased to 100% by changing the gas mixture to pure oxygen.

Throughout the experiment invasive physiological parameters RPP, RBF, cortical and medullary tissue pO_2 and Laser-flux were simultaneously monitored together with T_2*, T_2 and kidney size derived from MRI.

Data Processing and Analysis

Parametric maps of T_2* and T_2 were calculated by pixel-wise mono-exponential fitting to the signal intensities derived from a series of T_2* and T_2 weighted images acquired at different echo times (in-house developed program; MATLAB, R2010a, MathWorks, Natick, WA, USA).

Kidney movement throughout the experiment was corrected by image registration (FLIRT, FSL, www.fmrib.ox. ac.uk/fsl). For this purpose the first echo images of the multi echo MGE and MSME acquisitions were used. These images were registered onto the baseline scan. The resulting spatial transformation matrices were applied to the corresponding parametric maps.

For quantitative analysis of T_2* and T_2 regions of interest (ROIs) were defined according to the morphological features of the kidney. For this purpose, the layers (cortex (C), outer medulla (OM), inner medulla (IM)) were identified and measured in a series of freshly extracted rat kidneys [18]. The layers' dimensions were related to the individual kidney's length and width in the coronal view. From these measurements, a standardized model was derived that comprises a rectangular frame that tightly encloses the kidney and predefined sizes and positions of the ROIs relative to this frame such that the ROIs were accurately located within the respective layer (Figure 2). The positions of nine ROIs were defined: three ROIs in C (C1-C3), three ROIs in OM (O1-O3), and three ROIs in IM (I1-I3) as illustrated in Figure 2. The mean size of the ROIs was: C1, C3, O1, O3: 17 pixel, C2, O2: 46 pixel, I1, I3: 25 pixel, I2: 70 pixel. The segmentation software limited the operator interaction to the placement of a rectangular reference frame around the kidney. All ROIs were placed in safe

distance from the borders between these kidney layers to avoid any ‘contamination’ from the neighboring layers (partial segment effects) and to allow for inter-individual variations in morphology without the need to change the ROI position. The earlier described kidney segmentation model [18] was adapted for the current study to avoid overlap of the ROIs with the locations of the pO_2/Laser-flux probes (Fig. 2). Mean T_2* and T_2 values were calculated over the three ROIs placed in each kidney layer. The size of the reference rectangle, which tightly encloses the kidney, was used as an estimate for kidney size.

The invasively measured physiological data were averaged over the time period of the corresponding MR scans with the exception of the Laser-flux signals. Here 5s data intervals starting 1 s after the end of the MR acquisitions were used. This approach helped to exclude MR induced artifacts in the Laser-flux signals [12].

Statistical Analysis

To test our hypothesis the relation between invasively measured physiological parameters and parameters derived from MRI was assessed. For this purpose relative changes in the physiological parameters and in kidney size were tested for correlation with relative changes in T_2* and T_2 for all renal layers and for the three interventions. Spearman’s analysis (non-parametric correlation on ranks) was used, by which the strength of relationships is assessed that follow a monotonous function. If such a significant correlation was observed, additionally Pearson’s analysis (parametric correlation) was applied, by which the strength and parameters of linear relationships are assessed. A p-value $p<0.05$ was considered to be statistically relevant.

Results

Animal Preparation

Notwithstanding the experimental challenges dictated by the space constraints of the small bore MR scanner, surgical preparation was successfully performed in 15 out of 21 animals. The most frequent complication during surgery was unintended obstruction of renal blood flow caused by the vascular flow probe. To identify and exclude invalid data due to surgical, technical or physiological reasons all *in vivo* data were thoroughly examined. MR imaging scouts were used to check the positioning of the perivascular flow probe and the cortical and medullary Laser-flux/pO_2 probes. All renal T_2* maps were carefully checked for susceptibility artifacts induced by the surgical preparation or by the probes, which yielded data sets free of severe susceptibility artifacts for each renal layer for 15 animals. The invasively acquired physiological parameters were benchmarked against data and experience derived from our previous studies which included physiological measurements in large cohorts of animals [48-51].

Renal T_2* and T_2

Figure 3 shows exemplary T_2* and T_2 maps obtained during baseline, aortic occlusion, hypoxia, and hyperoxia together with ΔT_2* and ΔT_2 difference maps. The latter were determined by subtracting T_2* and T_2 maps acquired at the last time point of the intervention phase from baseline. **At baseline** the inner medulla including the papilla revealed T_2*/T_2 values that were markedly higher versus T_2*/T_2 observed for the cortex and outer medulla. Parametric maps showed a cortical intra-layer T_2*/T_2 pattern that indicates that the spatial resolution affords visualization of spatial variability in intra-layer pO_2, which is related to the distance to the vascular bundles [52, 53].

Hyperoxia induced rather uniform increase in renal T_2* and T_2 across the kidney as outlined by exemplary maps in Figure 3. Averaged over all animals maximum T_2* changes were 19±3% (C), 22±2% (OM), 7±4% (IM) and maximum T_2 changes were 7±1% (C), 9±1% (OM), 8±2% (IM). **Aortic occlusion** caused a T_2*/T_2 decrease for all renal layers. Averaged over all animals maximum T_2* changes were -11±2% (C), -42±2% (OM), -17±5% (IM) and maximum T_2 changes were -17±3% (C), -22±3% (OM), -6±6% (IM). **Hypoxia** induced

rather uniform reduction in renal T_2* and T_2 with maximum ΔT_2* -47±3% (C), -59±2% (OM), and -37±5% (IM)), and maximum ΔT_2 -28±3% (C), -36±4% (OM), and -20±6% (IM)).

Time Course of Physiological and MR Parameters during Interventions

Figure 4 outlines the time course of physiological and MR parameters monitored during **hyperoxia & recovery**. After onset of hyperoxia tissue pO_2 started to increase and reached 240% over baseline in the cortex and 60% over baseline in the medulla. This pO_2 increase was accompanied by small rises in RPP (7%) and RBF (8%). Laser-fluxes, renal conductance and kidney size remained largely unchanged. T_2* increased versus baseline with maxima of 19% in the cortex, 22% in the outer medulla, and 7% in the inner medulla. T_2 maps revealed smaller increases (C: 7%, OM: 9%, IM: 8%). After switching to normoxia tissue pO_2 slowly returned towards baseline. T_2* and T_2 returned to baseline more rapidly. RBF and RPP even fell somewhat below baseline.

Figure 5 illustrates the time course obtained for physiological and MR parameters during **aortic occlusion & recovery**. With onset of occlusion RBF immediately ceased and kidney size decreased by 3.9%. Tissue pO_2 rapidly decreased: within 90 seconds cortical pO_2 had dropped by 90% and medullary pO_2 by 97%. T_2* became also reduced, but much less than pO_2. T_2* displayed a different time course among the layers. Outer medullary T_2* declined instantly by 42% while cortical and inner medullary T_2* decreased only modestly by 11% and 17%. After onset of reperfusion cortical and inner medullary T_2* initially continued to decrease and reached a level of 71% of baseline in the cortex and 69% of baseline in the inner medulla before starting to re-increase. Excursions of T_2 were even smaller than those of T_2*. In response to the occluder's deflation RPP returned to baseline within 5 minutes while RBF's return to baseline was more slowly. Consequently renal conductance started significantly below baseline (not measurable during the occlusion) and slowly approximated baseline. Kidney size followed this trend and regained baseline within 8 minutes after reperfusion. Cortical and medullary pO_2 followed the gradual recovery of RBF and reached baseline level only 8 minutes into reperfusion. While cortical and tissue pO_2 started to improve immediately after onset of reperfusion, T_2* initially remained unchanged (OM) or was even further reduced (C, IM) before restoration to baseline values began.

Figure 6 depicts the time course obtained for physiological and MR parameters in response to the **hypoxia & recovery** maneuver. With the onset of hypoxia RPP declined by 46% and RBF decreased even more (by 70%). Renal conductance dropped by 53% and kidney size by 5%.

Tissue pO_2 gradually decreased: within 7 minutes of hypoxia medullary pO_2 had decreased by 96% and cortical pO_2 by 66%. T_2* and T_2 changes were found to be in sync with the pO_2 alterations. The drop in T_2* and T_2 observed during hypoxia was markedly larger than during occlusion. During hypoxia T_2* fell by 47% in C, 59% in OM, and 37% in IM. After switching to normoxia RPP, RBF, conductance and renal tissue pO_2 started to recover immediately and returned to baseline. The tissue hypoxia to normoxia transition was faster versus aortic occlusion-recovery. T_2* and pO_2 time courses slightly deviated during recovery from hypoxia as cortical and medullary pO_2 displayed some oscillations.

Correlations of Physiological and MR Parameters

Table 1 provides a synopsis of the correlations between physiological parameters and MR parameters in response to hyperoxia & recovery, occlusion & recovery, and hypoxia & recovery. Significant Spearman rank correlations between T_2* and tissue pO_2 were observed for all interventions and all renal layers as illustrated in Figures 7, 8, and 9. The weakest T_2*/pO_2 correlation was found during hyperoxia & recovery, a closer one in response to occlusion & recovery, and the closest T_2*/pO_2 correlation during hypoxia & recovery (Table 1). The inter-layer comparison revealed weakest T_2*/pO_2 correlations for the cortex (Figure 7) and closest correlations for the outer medulla (Figure 8).

Pearson's analysis revealed significant linear correlations of T_2* with outer medullary tissue pO_2 for all interventions. Cortical T_2* and pO_2 showed a significant linear correlation during occlusion & recovery only. This is plausible since the average O_2 saturation of Hb in most cortical vessels will be above 75% (i.e. in the non-linear range of the sigmoid oxyHb dissociation curve) under most conditions but not during the occlusion period, whereas saturation in medullary vessels will be lower (i.e., in the range of the curve that approaches linearity).

Significant Spearman correlations of T_2* to RBF were deduced for all renal layers and for all interventions (Figures 7-9). The closest correlation was observed for the outer medulla followed by the cortex and the inner medulla. The T_2*/RBF correlations for cortex and outer medulla were even superior to those between T_2* and tissue pO_2. The closest T_2*/RBF correlation occurred during hypoxia & recovery.

T_2*/RPP correlations were similar to T_2*/RBF correlations as outlined in Table 1. Surprisingly close correlations were observed between T_2* and kidney size during hypoxia & recovery and

for occlusion & recovery. In both cases, kidney size correlated well with renal vascular conductance (Table 2), as did renal vascular conductance with T_2* (Table 1). Significant correlations of RBF to tissue pO_2 were observed for all kidney layers during hypoxia & recovery and for occlusion & recovery (Table 2). These correlations were superior to the T_2*/pO_2 correlations observed for occlusion & recovery and hypoxia & recovery.

Discussion

Our results demonstrate that MR-PHYSIO is instrumental to detail the link between renal tissue pO_2 and T_2* *in vivo*. This is of essence to address the weakness of MRI, its qualitative nature, by benchmarking the surrogate MRI biomarkers against invasive methods while putting MRI's ability to non-invasively capture the physiological heterogeneity between and within the renal layers to good use. The technical challenges and practical obstacles of the MR environment were successfully offset. Remotely controlled standardized interventions were implemented in the MR scanner in order to systematically examine the validity and efficacy of parametric MRI as a surrogate marker for renal oxygenation. These efforts are of high relevance for research into the pathogenesis of renal diseases that are induced or promoted by renal tissue hypoperfusion and hypoxia.

Our findings indicate that changes in T_2* qualitatively reflect changes in renal tissue pO_2 induced by hyperoxia, aortic occlusion, and hypoxia. This is in alignment with the link between T_2*, O_2-saturation of Hb, blood pO_2, and tissue pO_2. A closer examination of the quantitative relation between relative changes in T_2* and in tissue pO_2 revealed discrepancies that point at factors other than the known shifts of the deoxyHb dissociation curve and changes in haematocrit, which may also confound the renal T_2*/ tissue pO_2 relationship. Major differences in the T_2*/pO_2 correlations together with the stark differences in the linear regression of T_2*/pO_2 indicate that simple translation of quantitative results obtained for one intervention of renal hemodynamics and oxygenation to another intervention is falling short from being appropriate. Also, taking the perfusion and oxygenation heterogeneity within any given kidney layer into account, extrapolation of results obtained for specific renal regions to other renal areas must be made with due caution.

Hyperoxia & recovery yielded weak correlations for tissue pO_2 changes versus T_2* changes for all kidney layers. This observation is plausible since almost all of the available Hb in arterial blood is already O_2 saturated under normoxic conditions. Increasing the inspiratory oxygen fraction to 100% barely lifts the O_2 saturation of Hb in arterial blood. It does substantially increase arterial blood pO_2 though, which enhances the driving force for O_2 diffusion from vessels to tissue so that renal tissue pO_2 increases dramatically. The difference in the pO_2 increase between cortex and medulla is likely due to arterio-venous diffusive O_2 shunting, which reduces the oxygen content of arterial blood that perfuses the medulla [3, 38, 52]. Benchmarked against the massive pO_2 increase T_2* changes were much smaller. Hyperoxia-induced increase of arterial blood oxygen content are barely detectable by T_2*-

mapping since the deoxyHb concentration is virtually unaffected. However, hyperoxia increases blood pO_2 in intrarenal veins due to increasing arterio-venous oxygen shunting in case of a higher arterio-venous pO_2 difference [3, 38]. As renal venous Hb is far from being completely saturated with O_2 under normoxic conditions hyperoxia induced increase in venous blood pO_2 translates into the small increase in T_2* observed in our study.

Aortic occlusion & recovery showed closer tissue pO_2/T_2* correlations for all renal layers versus those observed in response to hyperoxia & recovery. Occlusion of the suprarenal aorta results in abrupt cessation of blood flow into the kidney while renal O_2 consumption remains unaltered at this early stage. This leads to a rapid and massive decline in renal tissue pO_2, which reduces blood pO_2 and O_2 saturation of Hb in the intrarenal (micro-)vasculature. This intrarenal Hb deoxygenation is aggravated by a progressive rightward shift of the oxyHb dissociation curve during the occlusion due to intrarenal accumulation of CO_2. The increase in deoxyHb is reflected by the T_2* decrease observed during occlusion for all layers. The T_2* decrease was mild and slow as compared to the decline in pO_2 though, and displayed different characteristics for the kidney layers. These findings can be attributed to blood volume fraction changes which occurred during occlusion. While blood flow into kidney is abruptly stopped by the occlusion, outflow of blood via the renal vein will continue until pressures in intra-renal vessels and in the vena cava are equalized. This results in a reduction of intrarenal blood volume [54] and manifests itself in the immediate drop in kidney size shown here. Since the total volume of the other renal fluid compartments including the tubular, interstitial, and cellular fraction is probably largely unchanged, the blood volume fraction becomes markedly reduced. As T_2* is linked to the volume fraction of deoxyHb, the reduction in blood volume fraction compensates some of the increased deoxyHb blood concentration induced changes in T_2*. Consequently, the T_2* decrease turns out to be smaller than the actual change in blood (and tissue) oxygenation. It is plausible that this effect is much more pronounced in the cortex than in the medulla, due to the much larger blood volume in the cortex [4, 38]. T_2* in the cortex follows the declining blood (tissue) pO_2 less closely than in the outer medulla. The inner medulla's metabolism is largely anaerobic [55], hence the remaining oxygen in the stationary blood is sufficient for a longer time span so that pO_2 and T_2* decline only slowly.

By deflating the aortic occluder the kidney is reperfused. Complete restoration of RBF took about 8 minutes so that oxygen delivery recovers only gradually. At the same time, glomerular filtration, which was arrested during occlusion, is gradually restored. The ensuing restoration of tubular reabsorption necessitates higher O_2 consumption. Limited oxygen delivery and increased demand result in the observed slow recovery of tissue pO_2. The

substantial O_2 extraction from the freshly inflowing blood is embodied by a low T_2*. Although tissue pO_2 started to improve immediately after onset of reperfusion, cortical T_2* continued to decline even further before it started to recover. Again, this discrepancy most probably relies on a change in the blood volume fraction. With reperfusion renal blood volume increases while the total volume of the other fluid compartments is largely unchanged. Increased blood volume fraction at the onset of reperfusion leads T_2* to an overestimation of tissue hypoxia. The increase in blood volume is somewhat attenuated by renal vasoconstriction triggered by renal autoregulatory mechanisms [56], as evident from renal vascular conductance being significantly below baseline right after the onset of reperfusion. The attenuated recovery of intrarenal blood volume is also mirrored by the somewhat delayed restoration in kidney size.

Hypoxia & recovery revealed the strongest renal tissue pO_2/T_2* correlation for all interventions applied. Switching the inspiratory oxygen fraction to 8% resulted in arterial hypoxemia so that tissue pO_2 gradually decreased and reached a steady state. The major reason behind the pronounced decrease in medullary pO_2 is that the medulla is predominantly perfused by blood that had already traversed the cortex, where blood oxygen content is lowered by oxygen extraction and arterio-venous oxygen shunt diffusion [3, 4, 38, 52]. As expected, the pO_2 decrease during hypoxia was slower and with regard to the cortex also less pronounced than during aortic occlusion. In contrast, the T_2* response to hypoxia was significantly more pronounced versus aortic occlusion. It is evident that aortic occlusion must lower intrarenal blood oxygenation much more and faster than hypoxia. In addition, intrarenal pCO_2 increases during occlusion due to CO_2 accumulation, but decreases during hypoxia due to hyperventilation triggered by systemic hypoxemia [57]. Decreased pCO_2 shifts the deoxyHb dissociation curve to the left so that at given pO_2 the O_2 saturation of Hb is larger. Increased pCO_2 induces opposite effects. For all these reasons, T_2* decrease should be more pronounced during aortic occlusion versus hypoxia. Our results indicate that the T_2* response to FiO_2 8% overestimates the actual degree of blood (and tissue) hypoxia. The decrease in renal conductance during hypoxia suggests that renal vasoconstriction lowered intrarenal blood volume. Yet the vasoconstriction-related drop in renal blood volume during hypoxia is most likely smaller versus the outflow-induced drop during aortic occlusion. Intriguingly, the decrease in kidney size was somewhat larger during hypoxia than during occlusion. This observation points at an additional volume loss of renal tissue compartments other than blood. Contrary to aortic occlusion, where glomerular filtration ceases and with it the pressure gradient that drives tubular fluid toward the renal pelvis, filtration and tubular fluid flow will

decrease but not cease during hypoxia. The outflow lowers tubular volume. Moreover, reabsorbed fluid cannot be drained by peritubular capillaries during occlusion because of the arrested blood flow such that the sum of the tubular plus interstitial volumes remains constant. As peritubular capillary blood flow is not arrested during hypoxia, reabsorbed fluid is continued to be drained from the interstitium. Since the decrease in tubular volume is not counterbalanced by an increase in the interstitial volume, the sum of both volumes decreases. This translates into a larger decrease in the blood volume fraction during occlusion versus hypoxia which might explain the discrepancies in the T_2* and pO_2 response to hypoxia and aortic occlusion.

Significant rank correlations of RBF to T_2* were observed for all renal layers and for all interventions. These correlations were closer than those of tissue pO_2 to T_2* for the cortex and outer medulla. Tissue pO_2 primarily reflects the balance between O_2 supply and O_2 demand. Due to O_2 shunt diffusion, blood pO_2 in larger arterial and venous vessels exceeds that in capillaries and tissue pO_2. The amount of O_2 that is shunted depends on O_2 consumption but also on RBF and arterial O_2 content [3, 4, 38, 52]. In the cortex, the effect of changes in RBF on shunting appears to be enhanced: the correlations of RBF to cortical tissue pO_2 were much weaker than those of RBF and medullary tissue pO_2. When comparing RBF/T_2* versus pO_2/T_2* it should be taken into account that the pO_2 probes cover a rather small tissue volume ($r \approx 120$ µm) subjacent to the probes' tip [2, 12]. The individual position of a given probe in relation to larger vessels versus capillaries will therefore determine the individual absolute pO_2 values, and may also impinge on the relative changes during interventions. Unlike pO_2 measurements RBF measurements are unaffected by intrarenal spatial variabilities.

To summarize, this work presents valuable insights into the mechanisms behind alterations in renal T_2* by detailing the link between renal T_2* and renal tissue pO_2. Yet, a singular report eloquently refers to simultaneous measurements of renal R_2* (R_2* = 1/T_2*) and tissue pO_2 [47]. The authors modulated FiO_2 (range: 5-70%) in pigs and reported R_2*changes to be linearly related with pO_2 changes. This conclusion appears somewhat premature, since T_2* was measured in the contralateral kidney with the pO_2 probe being placed in the ipsilateral kidney. It should be also noted that correlation analysis was based upon group means rather than individual data pairs as used here.

The overall qualitative agreement of T_2* and pO_2 changes observed in the present study encourages further research into calibration of renal T_2* alterations using MR-PHYSIOL. Notwithstanding this success, our findings generated novel questions about the renal

T_2*/tissue pO_2 relation. It stands to reason that T_2* is directly related to the amount of deoxyHb per tissue volume and hence linked with tissue pO_2 via blood pO_2 and the oxyHb dissociation curve. However, the T_2* to tissue pO_2 correlation differences between the interventions and our renal vascular conductance and kidney size data indicate that changes in the blood volume fraction considerably influence renal T_2*. Renal vascular conductance changes point at changes in intrarenal blood volume that occur by passive circular distension induced by changes in the transmural pressure gradient, or by active vasomotion. Changes in kidney size may stem from volume changes in any of the renal fluid compartments. There are at least two compartments besides the vascular one that can experience rapid volume changes, which in turn modulate the blood volume fraction: the interstitial and the tubular compartment, with the latter being a particularity of the kidney. The tubular volume fraction is quite large and can rapidly change due (i) changes in filtration, (ii) alterations in tubular outflow towards the pelvis, (iii) modulation of the transmural pressure gradient, and (iv) changes in resorption. A recent report recognized that changes in blood volume fraction induced by changes in tubular volume may impact renal T_2* [17] by showing that the renal T_2* response indicated an increased oxygenation immediately after x-ray contrast agent administration rather than decreased oxygenation [17]. The dependence of $R_2=1/T_2$ on alterations in tubular volume has also been observed upon administration of vasoactive substances [58].

Unravelling the link between regional renal T_2* and tissue pO_2 - including the role of the T_2* confounding parameters vascular and tubular volume fraction and oxyHb dissociation curve - requires further research. Blood volume fraction, tubular volume fraction and oxyHb dissociation curve T_2* contributions must be differentiated from renal BOLD T_2* changes in order to provide quantitative means for interpretation of renal hemodynamics/oxygenation. These efforts should make use of the advanced capabilities of MR-PHYSIOL by including parallel imaging techniques to improve the temporal resolution [59-62], by investing into dual contrast techniques for simultaneous T_2*/T_2 weighted MRI [63], by driving T_2* mapping techniques free of image distortion [64] but also MR based assessment of renal blood volume [65] and by probing tubular volume fraction using diffusion weighted or intra-voxel incoherent motion techniques [43, 66-69], while blood sampling may be employed to examine the role of shifts in the oxyHb dissociation curve. These explorations are essential before the quantitative capabilities of parametric MRI can be translated from experimental research to improved clinical understanding of hemodynamics/oxygenation in kidney disorders.

References

1. Singh P, Ricksten SE, Bragadottir G, et al. Renal oxygenation and haemodynamics in acute kidney injury and chronic kidney disease. Clin Exp Pharmacol Physiol. 2013;40:138-47.
2. Evans RG, Gardiner BS, Smith DW, et al. Methods for studying the physiology of kidney oxygenation. Clin Exp Pharmacol Physiol. 2008;35:1405-12.
3. Evans RG, Goddard D, Eppel GA, et al. Factors that render the kidney susceptible to tissue hypoxia in hypoxemia. Am J Physiol Regul Integr Comp Physiol. 2011;300:R931-40.
4. Evans RG, Ince C, Joles JA, et al. Haemodynamic influences on kidney oxygenation: clinical implications of integrative physiology. Clin Exp Pharmacol Physiol. 2013;40:106-22.
5. Chawla LS, Kimmel PL. Acute kidney injury and chronic kidney disease: an integrated clinical syndrome. Kidney Int. 2012;82:516-24.
6. Seeliger E, Sendeski M, Rihal CS, et al. Contrast-induced kidney injury: mechanisms, risk factors, and prevention. Eur Heart J. 2012;33:2007-15.
7. Legrand M, Mik EG, Johannes T, et al. Renal hypoxia and dysoxia after reperfusion of the ischemic kidney. Mol Med. 2008;14:502-16.
8. Friederich-Persson M, Thorn E, Hansell P, et al. Kidney hypoxia, attributable to increased oxygen consumption, induces nephropathy independently of hyperglycemia and oxidative stress. Hypertension. 2013;62:914-9.
9. Hansell P, Welch WJ, Blantz RC, et al. Determinants of kidney oxygen consumption and their relationship to tissue oxygen tension in diabetes and hypertension. Clin Exp Pharmacol Physiol. 2013;40:123-37.
10. Prasad PV. Functional MRI of the kidney: tools for translational studies of pathophysiology of renal disease. Am J Physiol Renal Physiol. 2006;290:F958-74.
11. Evans RG, Leong CL, Anderson WP, et al. Don't be so BOLD: potential limitations in the use of BOLD MRI for studies of renal oxygenation. Kidney Int. 2007;71:1327-8; author reply 8.
12. Pohlmann A, Cantow K, Hentschel J, et al. Linking non-invasive parametric MRI with invasive physiological measurements (MR-PHYSIOL): towards a hybrid and integrated approach for investigation of acute kidney injury in rats. Acta Physiol (Oxf). 2013;207:673-89.
13. Prasad PV, Epstein FH. Changes in renal medullary pO2 during water diuresis as evaluated by blood oxygenation level-dependent magnetic resonance imaging: effects of aging and cyclooxygenase inhibition. Kidney Int. 1999;55:294-8.
14. Prasad PV, Priatna A, Spokes K, et al. Changes in intrarenal oxygenation as evaluated by BOLD MRI in a rat kidney model for radiocontrast nephropathy. J Magn Reson Imaging. 2001;13:744-7.
15. Li LP, Halter S, Prasad PV. Blood oxygen level-dependent MR imaging of the kidneys. Magn Reson Imaging Clin N Am. 2008;16:613-25, viii.
16. Haque M, Franklin T, Prasad P. Renal oxygenation changes during water loading as evaluated by BOLD MRI: effect of NOS inhibition. J Magn Reson Imaging. 2011;33:898-901.
17. Arakelyan K, Cantow K, Hentschel J, et al. Early effects of an x-ray contrast medium on renal T(2) */T(2) MRI as compared to short-term hyperoxia, hypoxia and aortic occlusion in rats. Acta Physiol (Oxf). 2013;208:202-13.
18. Pohlmann A, Hentschel J, Fechner M, et al. High temporal resolution parametric MRI monitoring of the initial ischemia/reperfusion phase in experimental acute kidney injury. PLoS One. 2013;8:e57411.
19. Peng XG, Bai YY, Fang F, et al. Renal Lipids and Oxygenation in Diabetic Mice: Noninvasive Quantification with MR Imaging. Radiology. 2013;269:748-57.

20. Morrell GR, Zhang JL, Lee VS. Science to Practice: Renal Hypoxia and Fat Deposition in Diabetic Neuropathy-New Insights with Functional Renal MR Imaging. Radiology. 2013;269:625-6.
21. Menzies RI, Zammit-Mangion A, Hollis LM, et al. An anatomically unbiased approach for analysis of renal BOLD magnetic resonance images. Am J Physiol Renal Physiol. 2013;305:F845-52.
22. Pruijm M, Hofmann L, Charollais-Thoenig J, et al. Effect of dark chocolate on renal tissue oxygenation as measured by BOLD-MRI in healthy volunteers. Clin Nephrol. 2013;80:211-7.
23. Pruijm M, Hofmann L, Vogt B, et al. Renal tissue oxygenation in essential hypertension and chronic kidney disease. Int J Hypertens. 2013;2013:696598.
24. Pruijm M, Hofmann L, Zanchi A, et al. Blockade of the renin-angiotensin system and renal tissue oxygenation as measured with BOLD-MRI in patients with type 2 diabetes. Diabetes Res Clin Pract. 2013;99:136-44.
25. Liss P, Cox EF, Eckerbom P, et al. Imaging of intrarenal haemodynamics and oxygen metabolism. Clin Exp Pharmacol Physiol. 2013;40:158-67.
26. Gloviczki ML, Lerman LO, Textor SC. Blood oxygen level-dependent (BOLD) MRI in renovascular hypertension. Curr Hypertens Rep. 2011;13:370-7.
27. Rognant N, Lemoine S, Laville M, et al. [Evaluation of renal oxygen content by BOLD MRI]. Nephrol Ther. 2012;8:212-5.
28. Park SY, Kim CK, Park BK, et al. Evaluation of transplanted kidneys using blood oxygenation level-dependent MRI at 3 T: a preliminary study. AJR Am J Roentgenol. 2012;198:1108-14.
29. Donati OF, Nanz D, Serra AL, et al. Quantitative BOLD response of the renal medulla to hyperoxic challenge at 1.5 T and 3.0 T. NMR Biomed. 2012;25:1133-8.
30. Ebrahimi B, Gloviczki M, Woollard JR, et al. Compartmental analysis of renal BOLD MRI data: introduction and validation. Invest Radiol. 2012;47:175-82.
31. Chrysochou C, Mendichovszky IA, Buckley DL, et al. BOLD imaging: a potential predictive biomarker of renal functional outcome following revascularization in atheromatous renovascular disease. Nephrol Dial Transplant. 2012;27:1013-9.
32. Rognant N, Guebre-Egziabher F, Bacchetta J, et al. Evolution of renal oxygen content measured by BOLD MRI downstream a chronic renal artery stenosis. Nephrol Dial Transplant. 2011;26:1205-10.
33. Warner L, Glockner JF, Woollard J, et al. Determinations of renal cortical and medullary oxygenation using blood oxygen level-dependent magnetic resonance imaging and selective diuretics. Invest Radiol. 2011;46:41-7.
34. Gloviczki ML, Glockner J, Gomez SI, et al. Comparison of 1.5 and 3 T BOLD MR to study oxygenation of kidney cortex and medulla in human renovascular disease. Invest Radiol. 2009;44:566-71.
35. Rossi C, Sharma P, Pazahr S, et al. Blood oxygen level-dependent magnetic resonance imaging of the kidneys: influence of spatial resolution on the apparent R2* transverse relaxation rate of renal tissue. Invest Radiol. 2013;48:671-7.
36. Ogawa S. Finding the BOLD effect in brain images. Neuroimage. 2012;62:608-9.
37. Griffeth VE, Buxton RB. A theoretical framework for estimating cerebral oxygen metabolism changes using the calibrated-BOLD method: modeling the effects of blood volume distribution, hematocrit, oxygen extraction fraction, and tissue signal properties on the BOLD signal. Neuroimage. 2011;58:198-212.
38. Evans RG, Gardiner BS, Smith DW, et al. Intrarenal oxygenation: unique challenges and the biophysical basis of homeostasis. Am J Physiol Renal Physiol. 2008;295:F1259-70.
39. Michaely HJ, Metzger L, Haneder S, et al. Renal BOLD-MRI does not reflect renal function in chronic kidney disease. Kidney Int. 2012;81:684-9.

40. Fine LG, Dharmakumar R. Limitations of BOLD-MRI for assessment of hypoxia in chronically diseased human kidneys. Kidney Int. 2012;82:934-5; author reply 5.
41. Inoue T, Kozawa E, Okada H, et al. Is there no future for renal BOLD-MRI? Kidney Int. 2012;82:934; author reply 5.
42. Dean DA, Jia CX, Cabreriza SE, et al. Validation study of a new transit time ultrasonic flow probe for continuous great vessel measurements. ASAIO journal (American Society for Artificial Internal Organs : 1992). 1996;42:M671-6.
43. Hueper K, Rong S, Gutberlet M, et al. T2 relaxation time and apparent diffusion coefficient for noninvasive assessment of renal pathology after acute kidney injury in mice: comparison with histopathology. Invest Radiol. 2013;48:834-42.
44. Juillard L, Lerman LO, Kruger DG, et al. Blood oxygen level-dependent measurement of acute intra-renal ischemia. Kidney Int. 2004;65:944-50.
45. dos Santos EA, Li L-P, Ji L, et al. Early changes with diabetes in renal medullary hemodynamics as evaluated by fiberoptic probes and BOLD magnetic resonance imaging. Investigative radiology. 2007;42:157-62.
46. Li L-P, Ji L, Santos EA, et al. Effect of nitric oxide synthase inhibition on intrarenal oxygenation as evaluated by blood oxygenation level-dependent magnetic resonance imaging. Investigative radiology. 2009;44:67-73.
47. Pedersen M, Dissing T, Morkenborg J, et al. Validation of quantitative BOLD MRI measurements in kidney: Application to unilateral ureteral obstruction. Kidney Int. 2005;67:2305-12.
48. Flemming B, Seeliger E, Wronski T, et al. Oxygen and renal hemodynamics in the conscious rat. J Am Soc Nephrol. 2000;11:18-24.
49. Hoff U, Lukitsch I, Chaykovska L, et al. Inhibition of 20-HETE synthesis and action protects the kidney from ischemia/reperfusion injury. Kidney Int. 2011;79:57-65.
50. Seeliger E, Flemming B, Wronski T, et al. Viscosity of contrast media perturbs renal hemodynamics. J Am Soc Nephrol. 2007;18:2912-20.
51. Seeliger E, Cantow K, Arakelyan K, et al. Low-Dose Nitrite Alleviates Early Effects of an X-ray Contrast Medium on Renal Hemodynamics and Oxygenation in Rats. Invest Radiol. 2013. [epub ahead]
52. Schurek HJ. [Kidney medullary hypoxia: a key to understanding acute renal failure?]. Klin Wochenschr. 1988;66:828-35.
53. Lubbers DW, Baumgartl H. Heterogeneities and profiles of oxygen pressure in brain and kidney as examples of the pO2 distribution in the living tissue. Kidney Int. 1997;51:372-80.
54. Grosenick D, Steinkellner O, Wabnitz H, et al. Near-infrared spectroscopy of renal tissue in vivo. Proc of SPIE. 2013.
55. Edwards A, Silldforff EP, Pallone TL. The renal medullary microcirculation. Front Biosci. 2000;5:E36-52.
56. Seeliger E, Wronski T, Ladwig M, et al. The renin-angiotensin system and the third mechanism of renal blood flow autoregulation. Am J Physiol Renal Physiol. 2009;296:F1334-45.
57. Marshall JM, Metcalfe JD. Influences on the cardiovascular response to graded levels of systemic hypoxia of the accompanying hypocapnia in the rat. J Physiol. 1989;410:381-94.
58. Storey P, Ji L, Li LP, et al. Sensitivity of USPIO-enhanced R2 imaging to dynamic blood volume changes in the rat kidney. J Magn Reson Imaging. 2011;33:1091-9.
59. Niendorf T, Sodickson DK. Highly accelerated cardiovascular MR imaging using many channel technology: concepts and clinical applications. Eur Radiol. 2008;18:87-102.
60. Niendorf T, Sodickson DK. Parallel imaging in cardiovascular MRI: methods and applications. NMR Biomed. 2006;19:325-41.

61. Niendorf T, Saranathan M, Lingamneni A, et al. Short breath-hold, volumetric coronary MR angiography employing steady-state free precession in conjunction with parallel imaging. Magn Reson Med. 2005;53:885-94.
62. Niendorf T, Sodickson D. [Acceleration of cardiovascular MRI using parallel imaging: basic principles, practical considerations, clinical applications and future directions]. Rofo. 2006;178:15-30.
63. Fuchs K, Hezel F, Klix S, et al. Simultaneous dual contrast weighting using double echo rapid acquisition with relaxation enhancement (RARE) imaging. Magn Reson Med. 2013.[epub ahead]
64. Heinrichs U, Utting JF, Frauenrath T, et al. Myocardial T2* mapping free of distortion using susceptibility-weighted fast spin-echo imaging: a feasibility study at 1.5 T and 3.0 T. Magn Reson Med. 2009;62:822-8.
65. Wang F, Jiang RT, Tantawy MN, et al. Repeatability and sensitivity of high resolution blood volume mapping in mouse kidney disease. J Magn Reson Imaging. 2013.
66. Eckerbom P, Hansell P, Bjerner T, et al. Intravoxel incoherent motion MR imaging of the kidney: pilot study. Adv Exp Med Biol. 2013;765:55-8.
67. Zhang JL, Sigmund EE, Rusinek H, et al. Optimization of b-value sampling for diffusion-weighted imaging of the kidney. Magn Reson Med. 2012;67:89-97.
68. Ichikawa S, Motosugi U, Ichikawa T, et al. Intravoxel incoherent motion imaging of the kidney: alterations in diffusion and perfusion in patients with renal dysfunction. Magn Reson Imaging. 2013;31:414-7.
69. Niendorf T, Dijkhuizen RM, Norris DG, et al. Biexponential diffusion attenuation in various states of brain tissue: implications for diffusion-weighted imaging. Magn Reson Med. 1996;36:847-57.

Figure Captions

Figure 1:

Coronal T_2* weighted image of a rat kidney (**left**) used for control of the perivascular flow probe and the cortical and medullary Laser-flux/pO_2 probes position during the *in vivo* experiments. For this purpose the imaging slice was positioned such that both probes were located within the imaging plane. The T_2*map obtained for the same coronal view of the kidney map (**middle**) also shows the position of the perivascular flow probe and the cortical and medullary Laser-flux/pO_2 probes. Schematic view of the positions used for the perivascular flow probe and the cortical and medullary Laser-flux/pO_2 probes **(right)**.

Figure 2:

Kidney segmentation model overlaid onto a photograph of a freshly excised rat kidney in coronal view (**A**) and superimposed to a T_2*-map of a rat kidney (**B**). During analysis the rectangular reference frame is manually positioned around the kidney, followed by an automated drawing of the diagonals (yellow). After their intersections with the kidney borders are defined manually, the ROIs (I1-I2, O1-O3, C1-C3, I: inner medulla, O: outer medulla, C: cortex) are automatically placed at pre-defined relative positions with regard to these references. The numbers shown on the horizontal and vertical axis as well as on the diagonals signify percentages of the reference frame dimensions and of the diagonals.

Figure 3:

A,B) Examples of renal T_2* maps (**A**) and T_2 maps (**B**) derived from baseline and during aortic occlusion, hypoxia and hyperoxia. **C,D)** Corresponding ΔT_2* (**C**) and ΔT_2 (**D**) maps which represent the pixel-by-pixel T_2* and T_2 difference between the last time point of each intervention phase and baseline.

Figure 4:

Time courses of physiological and MR parameters throughout baseline, hyperoxia and recovery: relative changes of RPP (n=15), RBF (n=10), renal conductance (n=10), kidney size (n=15), cortical/medullary Laser-flux (n=11/13), cortical/medullary pO_2 (n=12/10), cortical/outer medullary/inner medullary T_2* (n=15/15/15), and cortical/outer medullary/inner medullary T_2 (n=14/15/14). Hyperoxia started at t = 0. Its duration is indicated by the grey shading. Absolute parameter values at baseline are used to provide quantitative guidance.

Figure 5:

Time courses of physiological and MR parameters throughout baseline, aortic occlusion and recovery: relative changes of RPP (n=15), RBF (n=10), renal conductance (n=10), kidney size (n=15), cortical/medullary Laser-flux (n=12/13), cortical/medullary pO_2 (n=12/9), cortical/outer medullary/inner medullary T_2* (n=15/15/15), and cortical/outer medullary/inner medullary T_2 (n=14/15/14). Aortic occlusion started at t = 0. Its duration is indicated by the grey shading. Absolute parameter values at baseline are used to provide quantitative guidance.

Figure 6:

Time courses of physiological and MR parameters throughout baseline, hypoxia and recovery: relative changes of RPP (n=13), RBF (n=8), renal conductance (n=8), kidney size (n=13), cortical/medullary Laser-flux (n=11/13), cortical/medullary pO_2 (n=9/8), cortical/outer medullary/inner medullary T_2* (n=13/13/13), and cortical/outer medullary/inner medullary T_2 (n=12/13/12). Hypoxia started at t = 0. Its duration is indicated by the grey shading. In two rats the hypotensive response was so pronounced that hypoxia had to be stopped prematurely, therefore their data are not included here. Absolute parameter values at baseline are used to provide quantitative guidance.

Figure 7:

Parametric correlation analysis (Pearson's analysis) between relative changes of cortical T_2* and relative changes of cortical pO_2 (**left**) or renal blood flow (**right**) for aortic occlusion & recovery (**top**), hypoxia & recovery (**center**) and hyperoxia & recovery (**bottom**). The coefficient of determination for Pearson (R_p^2) is given together with the Spearman coefficient

(R_s^2); ** denotes $p<0.01$ The linear regression curve is shown only for significant Pearson's correlations of $p<0.05$.

Figure 8:

Parametric correlation analysis (Pearson's analysis) between relative changes of outer medullary T_2* and relative changes of medullary pO_2 (**left**) or renal blood flow (**right**) for aortic occlusion & recovery (**top**), hypoxia & recovery (**center**) and hyperoxia & recovery (**bottom**). The coefficient of determination for Pearson (R_p^2) is given together with the Spearman coefficient (R_s^2); ** denotes $p<0.01$.

Figure 9:

Parametric correlation analysis (Pearson's analysis) between relative changes of inner medullary T_2* and relative changes of medullary pO_2 (**left**) or renal blood flow (**right**) for aortic occlusion & recovery (**top**), hypoxia & recovery (**center**) and hyperoxia & recovery (**bottom**). The coefficient of determination for Pearson (R_p^2) is given together with the Spearman coefficient (R_s^2); * denotes $p<0.05$, ** denotes $p<0.01$. The linear regression curve is shown only for significant Pearson's correlations of $p<0.05$.

Table 1

Hyperoxia & Recovery

		R^2_s	R^2_p	f(x) = m x + n	
				m	n
	C	0.14**	0.01		
T_2* vs pO_2	OM	0.19**	0.16**	0.16	0.88
	IM	0.21**	0.13**	0.16	0.88
	C	0.43**	0.50**	0.84	0.24
T_2* vs RBF	OM	0.43**	0.50**	0.92	0.18
	IM	0.17**	0.18**	0.51	0.53
	C	0.50**	0.49**	0.92	0.16
T_2* vs RPP	OM	0.40**	0.43**	1.01	0.1
	IM	0.10**	0.06*	0.36	0.69
	C	0.28**	0.28**	-0.39	1.45
T_2* vs Laser-flux	OM	0.02	0.01		
	IM	0.05*	0.03		
	C	0.24**	0.26**	4.87	-3.81
T_2* vs kidney size	OM	0.24**	0.27**	5.72	-4.64
	IM	0.11**	0.09**	3.12	-2.08
	C	0.00	0.00		
T_2* vs conductance	OM	0.01	0.00		
	IM	0.00	0.00		

Occlusion & Recovery

		R^2_s	R^2_p	f(x) = m x + n	
				m	n
	C	0.24**	0.23**	0.13	0.83
T_2* vs pO_2	OM	0.54**	0.59**	0.4	0.56
	IM	0.28**	0.24**	0.23	0.71
	C	0.33**	0.18**	0.16	0.78
T_2* vs RBF	OM	0.66**	0.58**	0.41	0.49
	IM	0.09*	0.06		
	C	0.32**	0.14**	0.15	0.78
T_2* vs RPP	OM	0.60**	0.53**	0.45	0.41
	IM	0.10**	0.07*	0.15	0.73
	C	0.02	0.03		
T_2* vs Laser-flux	OM	0.44**	0.45**	0.32	0.54
	IM	0.03	0.02		
	C	0.45**	0.38**	3.68	-2.71
T_2* vs kidney size	OM	0.54**	0.45**	6.17	-5.28
	IM	0.13**	0.12**	2.83	-1.92
	C	0.55**	0.35**	0.58	0.42
T_2* vs conductance	OM	0.45**	0.10*	0.85	0.11
	IM	0.17*	0.34**	0.50	0.46

Hypoxia & Recovery

		R^2_s	R^2_p	f(x) = m x + n	
				m	n
T_2* vs pO_2	**C**	0.25**	0.03		
	OM	0.67**	0.67**	0.43	0.44
	IM	0.60**	0.63**	0.33	0.59
T_2* vs RBF	**C**	0.74**	0.74**	0.59	0.38
	OM	0.84**	0.81**	0.74	0.21
	IM	0.53**	0.49**	0.44	0.51
T_2* vs RPP	**C**	0.77**	0.74**	0.98	-0.02
	OM	0.64**	0.68**	1.14	-0.23
	IM	0.41**	0.36**	0.62	0.33
T_2* vs Laser-flux	**C**	0.03	0.01		
	OM	0.05	0.07		
	IM	0.01	0.00		
T_2* vs kidney size	**C**	0.55**	0.43**	4.65	-3.75
	OM	0.57**	0.40**	5.48	-4.63
	IM	0.39**	0.31**	3.57	-2.64
T_2* vs conductance	**C**	0.27**	0.34**	0.51	0.39
	OM	0.44**	0.47**	0.71	0.16
	IM	0.27**	0.27**	0.42	0.49

Table 1:

Summary of the coefficients of determination for correlation analyses of MR versus physiological parameters according to Spearman (R^2_s) and Pearson (R^2_p) for three interventions (hyperoxia & recovery, aortic occlusion & recovery, hypoxia & recovery) and three kidney layers (C = cortex, OM = outer medulla, IM = inner medulla); *****: significant correlations with $p<0.05$, ******: significant correlations with $p<0.01$. The slope (m) and intercept (n) of the linear regression equations are shown for significant Pearson's correlations at $p<0.05$.

Table 2

Hyperoxia & Recovery

		R^2_s	R^2_p	f(x) = m x + n	
				m	n
RBF vs pO_2	**C**	0.15**	0.04*	2.56	-0.25
	M	0.26**	0.12**	1.27	-0.1
RBF vs Laser-flux	**C**	0.20**	0.28**	-0.68	1.74
	M	0.01	0.00		
Laser-flux vs pO_2	**C**	0.00	0.01		
	M	0.04*	0.02		
Kidney size vs Conductance		0.03	0.06		

Occlusion & Recovery

		R^2_s	R^2_p	f(x) = m x + n	
				m	n
RBF vs pO_2	**C**	0.46**	0.43**	0.78	0.08
	M	0.68**	0.58**	0.8	0.11
RBF vs Laser-flux	**C**	0.10**	0.20**	0.68	0.45
	M	0.62**	0.69**	1.04	0.09
Laser-flux vs pO_2	**C**	0.05**	0.08**	0.26	0.46
	M	0.27**	0.32**	0.5	0.25
Kidney size vs Conductance		0.46**	0.37**	0.08	0.92

Hypoxia & Recovery

		R^2_s	R^2_p	f(x) = m x + n	
				m	n
RBF vs pO_2	**C**	0.27**	0.02		
	M	0.86**	0.79**	1.34	-0.3
RBF vs Laser-flux	**C**	0.14**	0.12**	0.4	0.44
	M	0.07*	0.18**	0.42	0.44
Laser-flux vs pO_2	**C**	0.02	0.01		
	M	0.06*	0.03		
Kidney size vs Conductance		0.45**	0.43**	0.10	0.90

Table 2:

Summary of the coefficients of determination for correlation analyses of physiological parameters according to Spearman (R^2_s) and Pearson (R^2_p) for three interventions (hyperoxia & recovery, aortic occlusion & recovery, hypoxia & recovery) and two kidney layers (C=cortex, M=medulla); *****: significant correlations with $p<0.05$, ******: significant correlations

with $p<0.01$. The slope (m) and intercept (n) of the linear regression equations are shown for significant Pearson's correlations at $p<0.05$.

Figure 1
Click here to download high resolution image

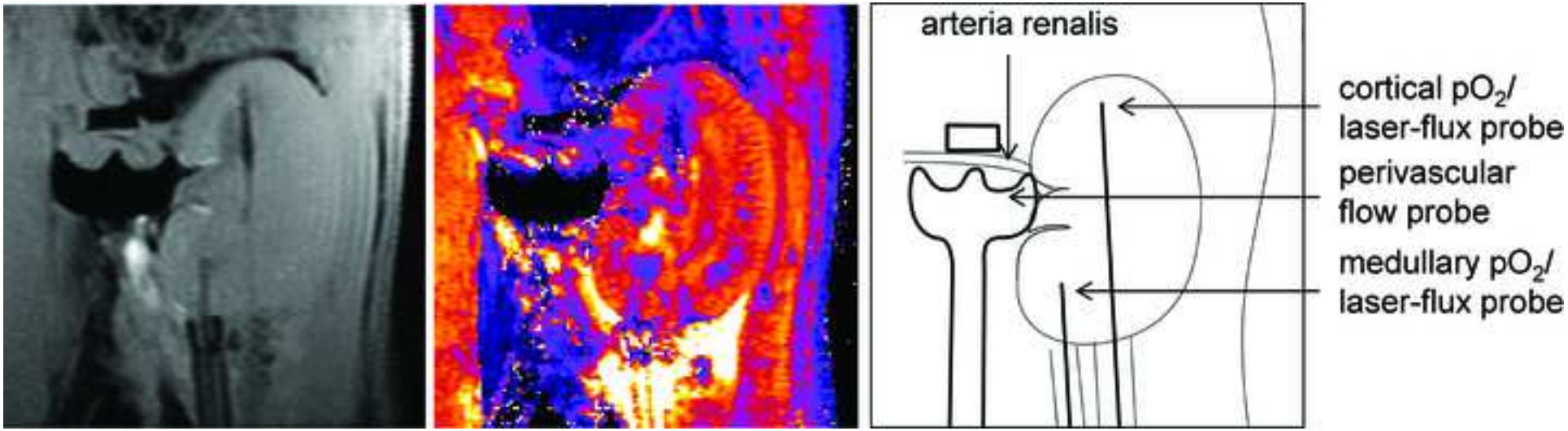

Figure 2 revised

Click here to download high resolution image

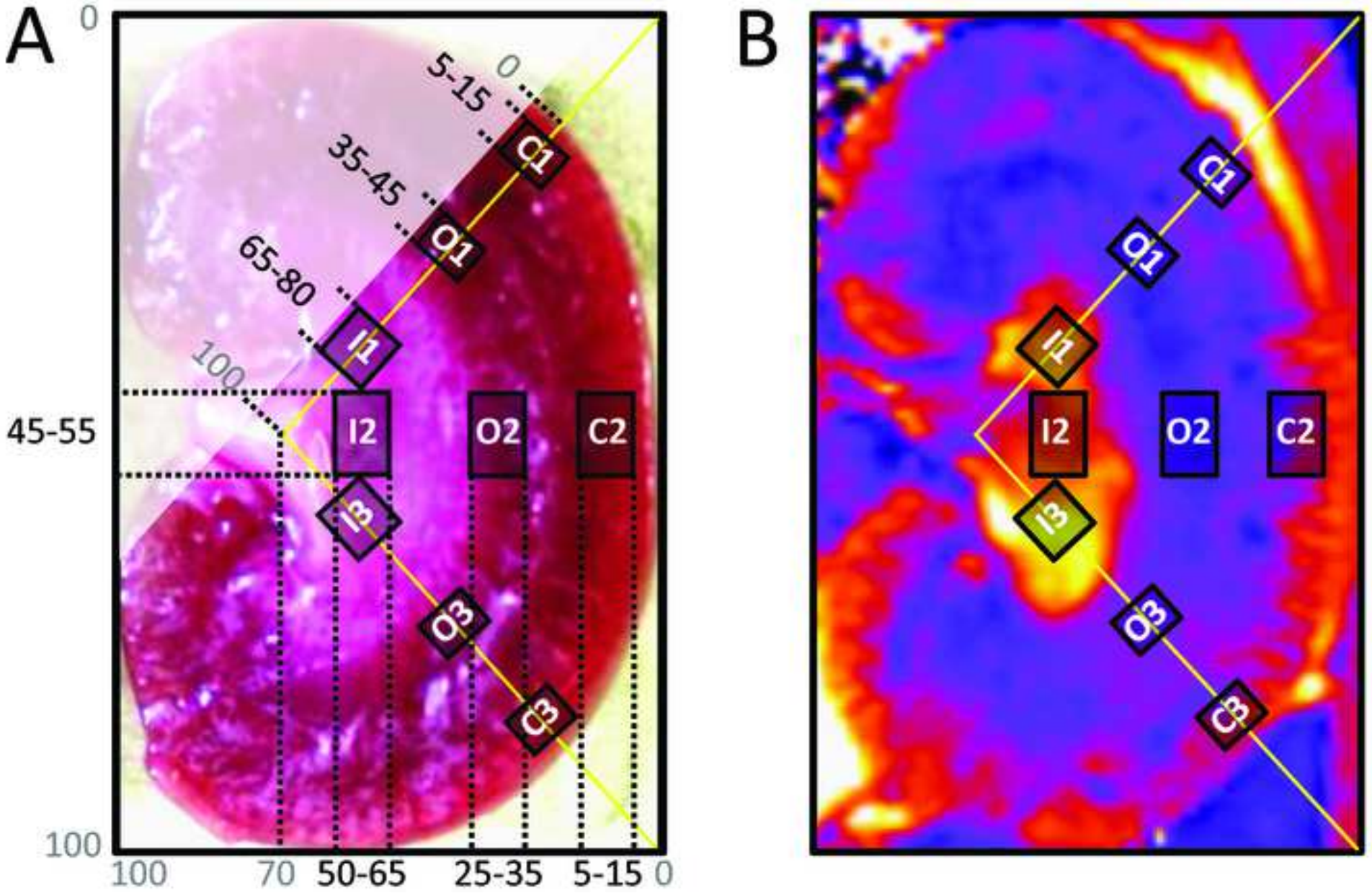

Figure 3
Click here to download high resolution image

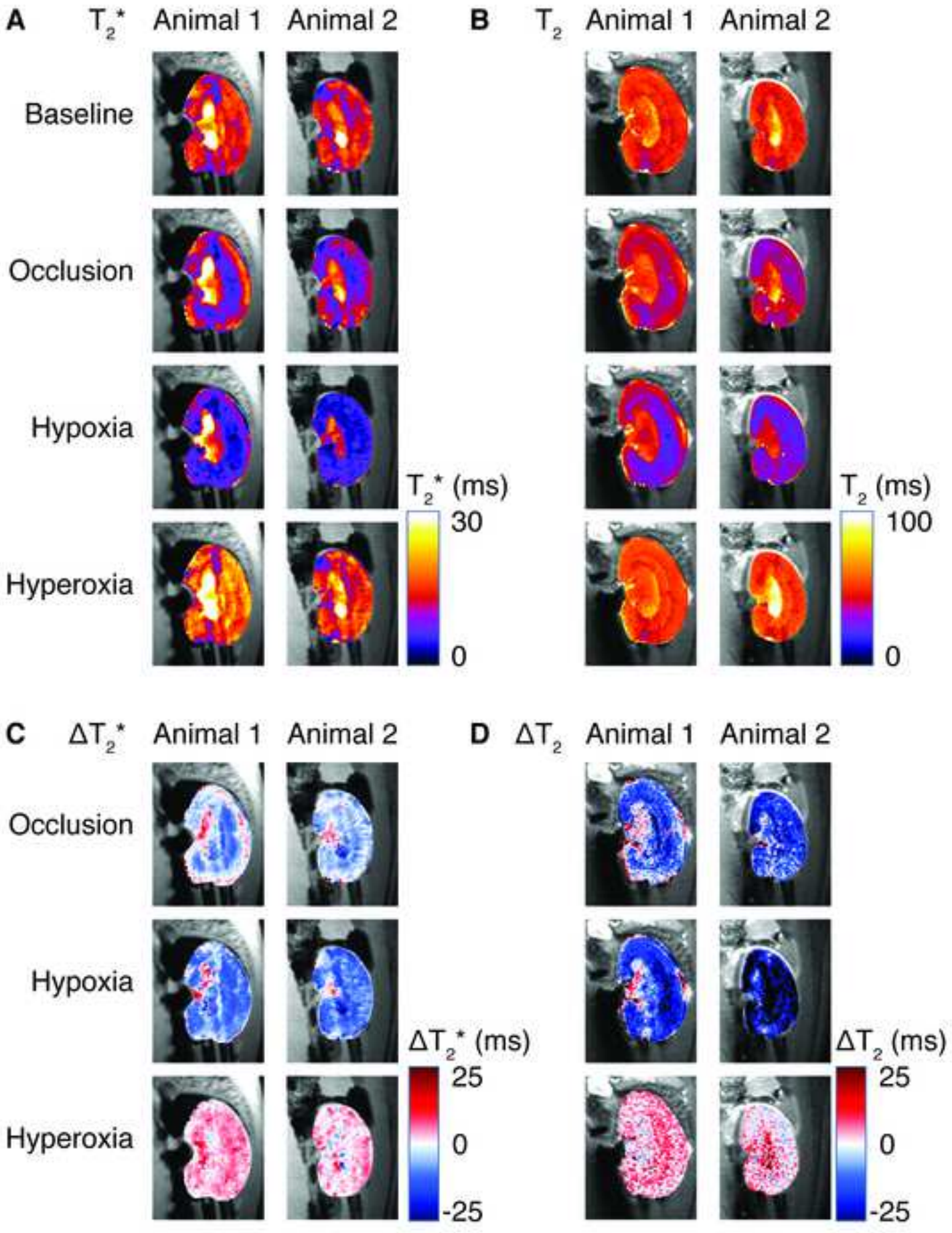

Figure 4

Click here to download high resolution image

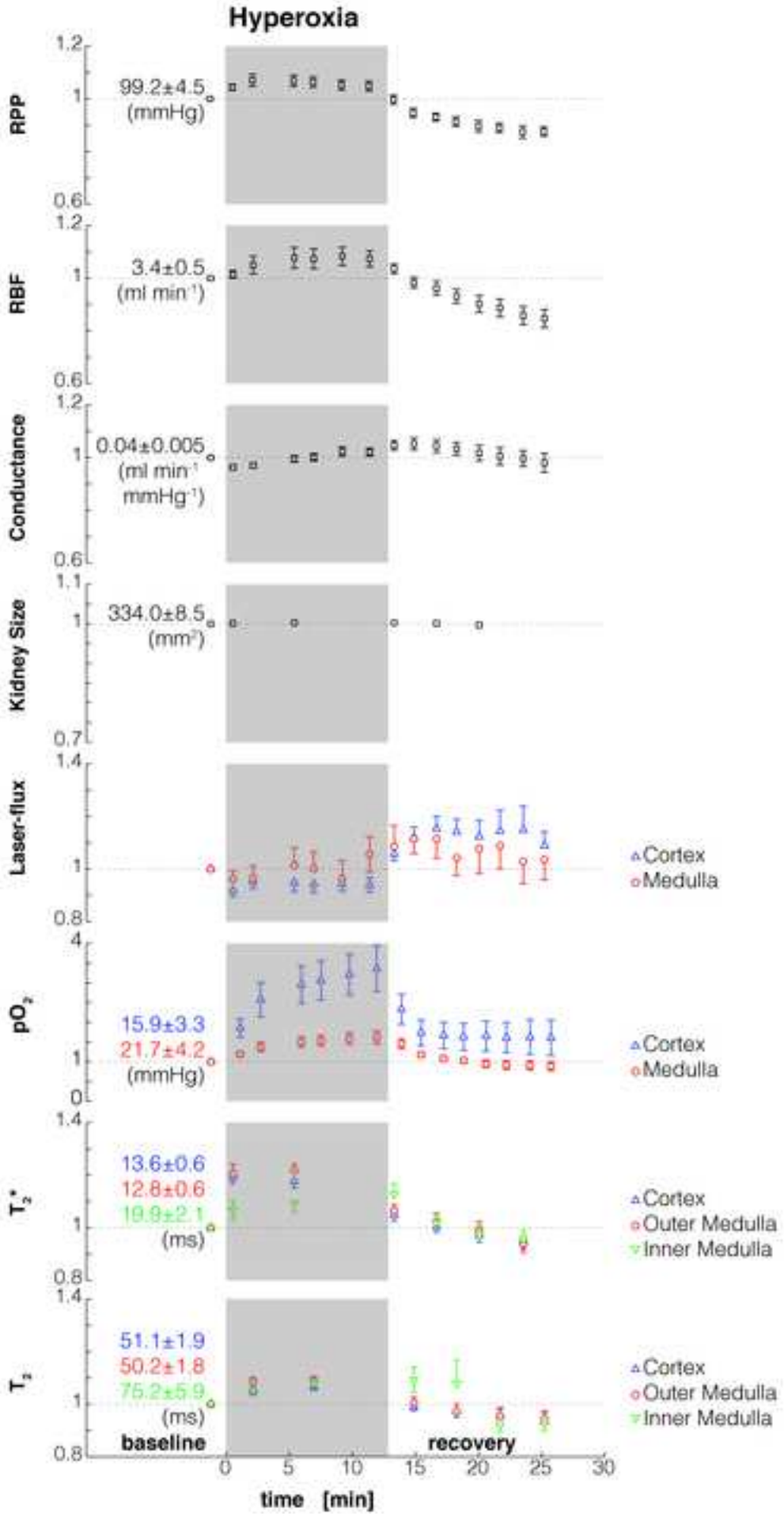

Figure 5
Click here to download high resolution image

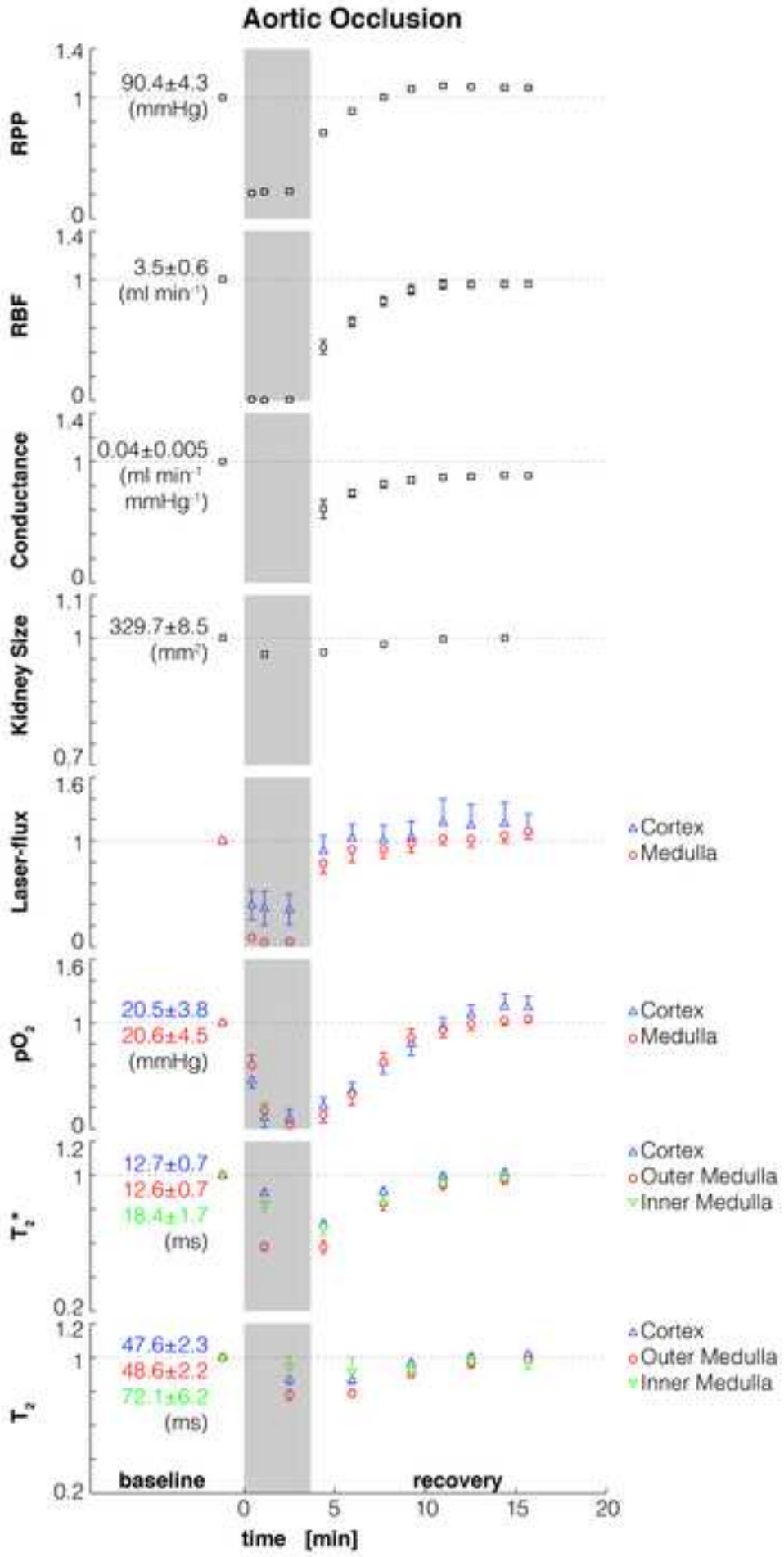

Figure 6

Click here to download high resolution image

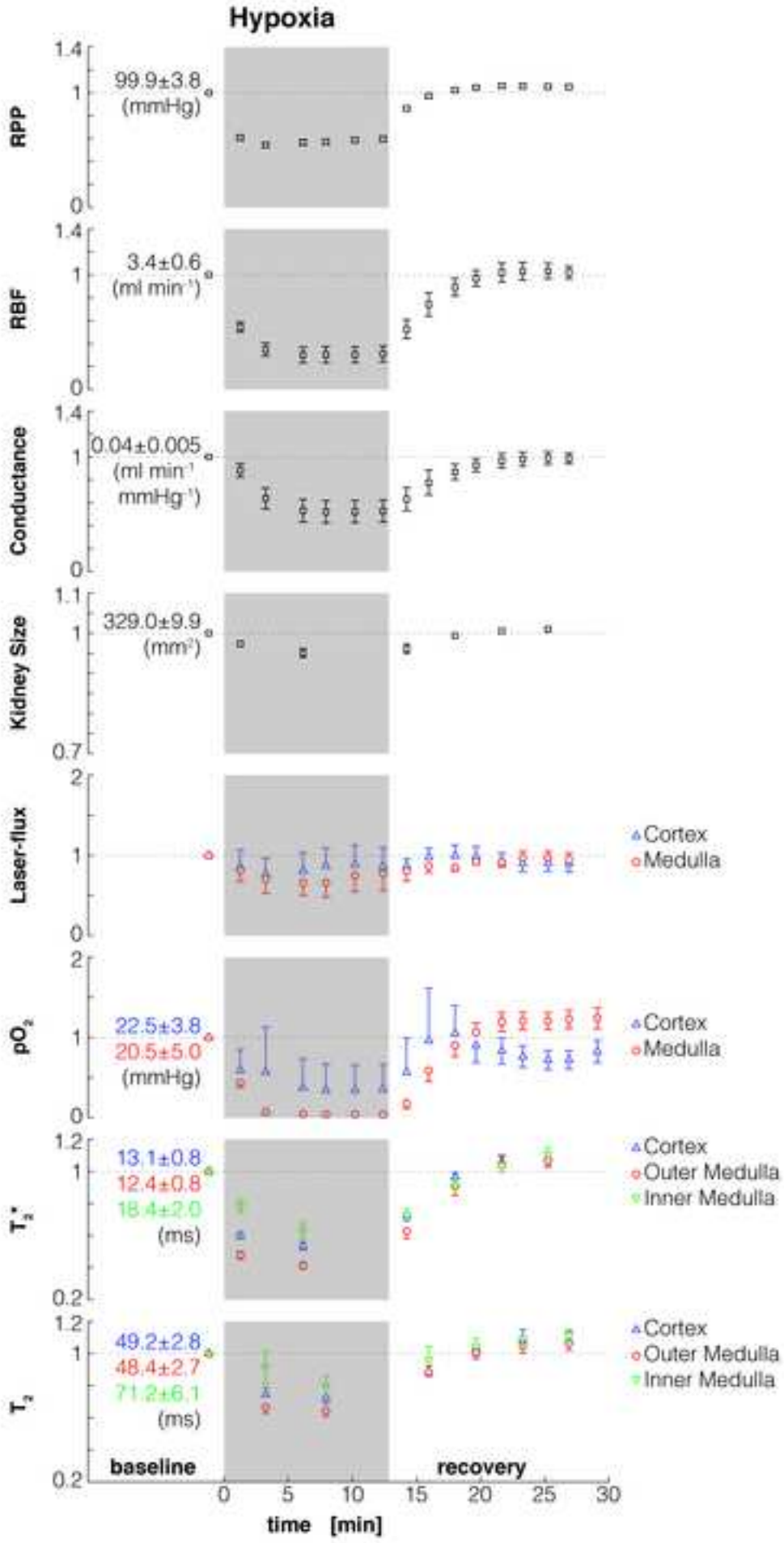

Figure 7 revised
Click here to download high resolution image

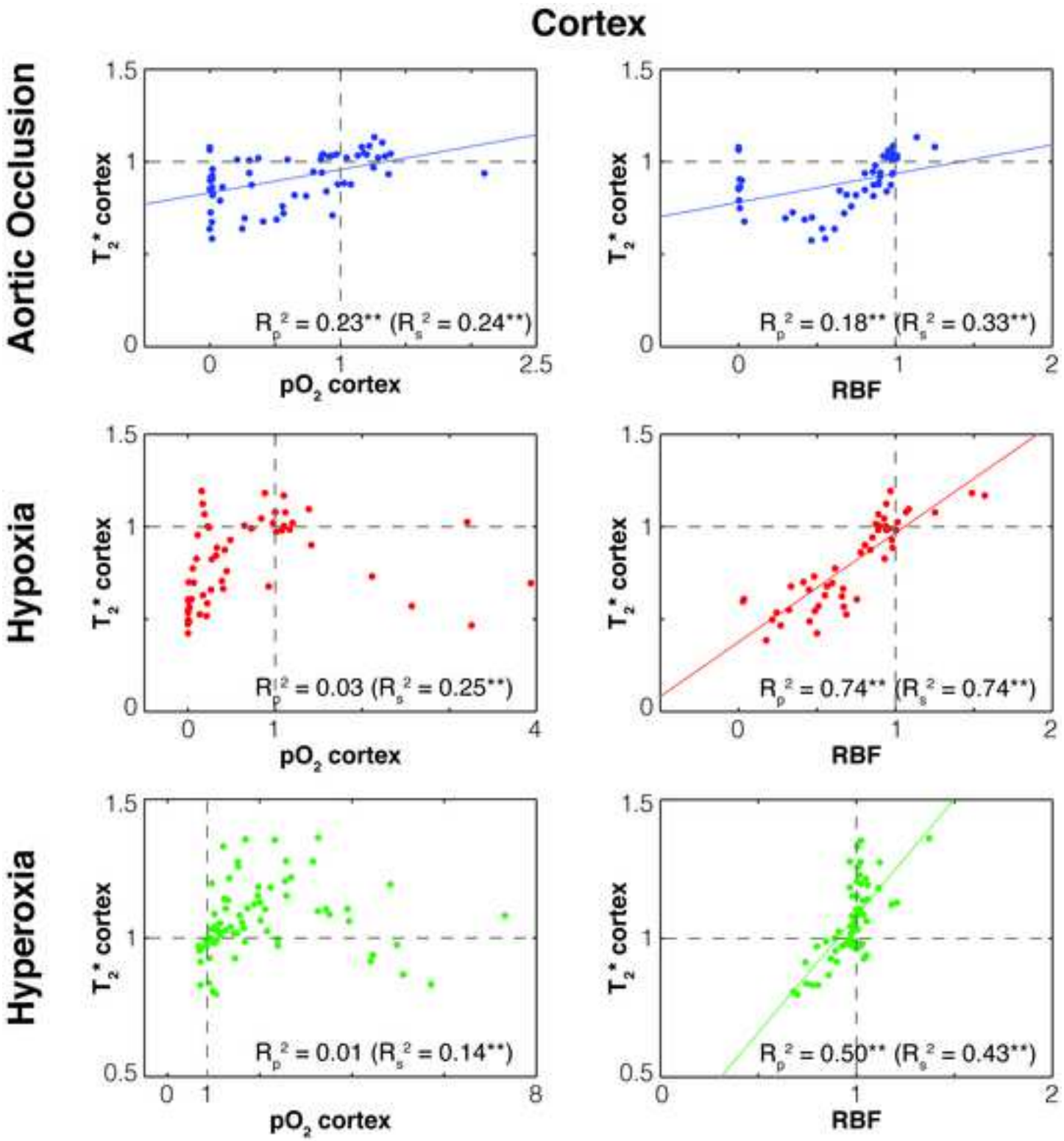

Figure 8 revised
Click here to download high resolution image

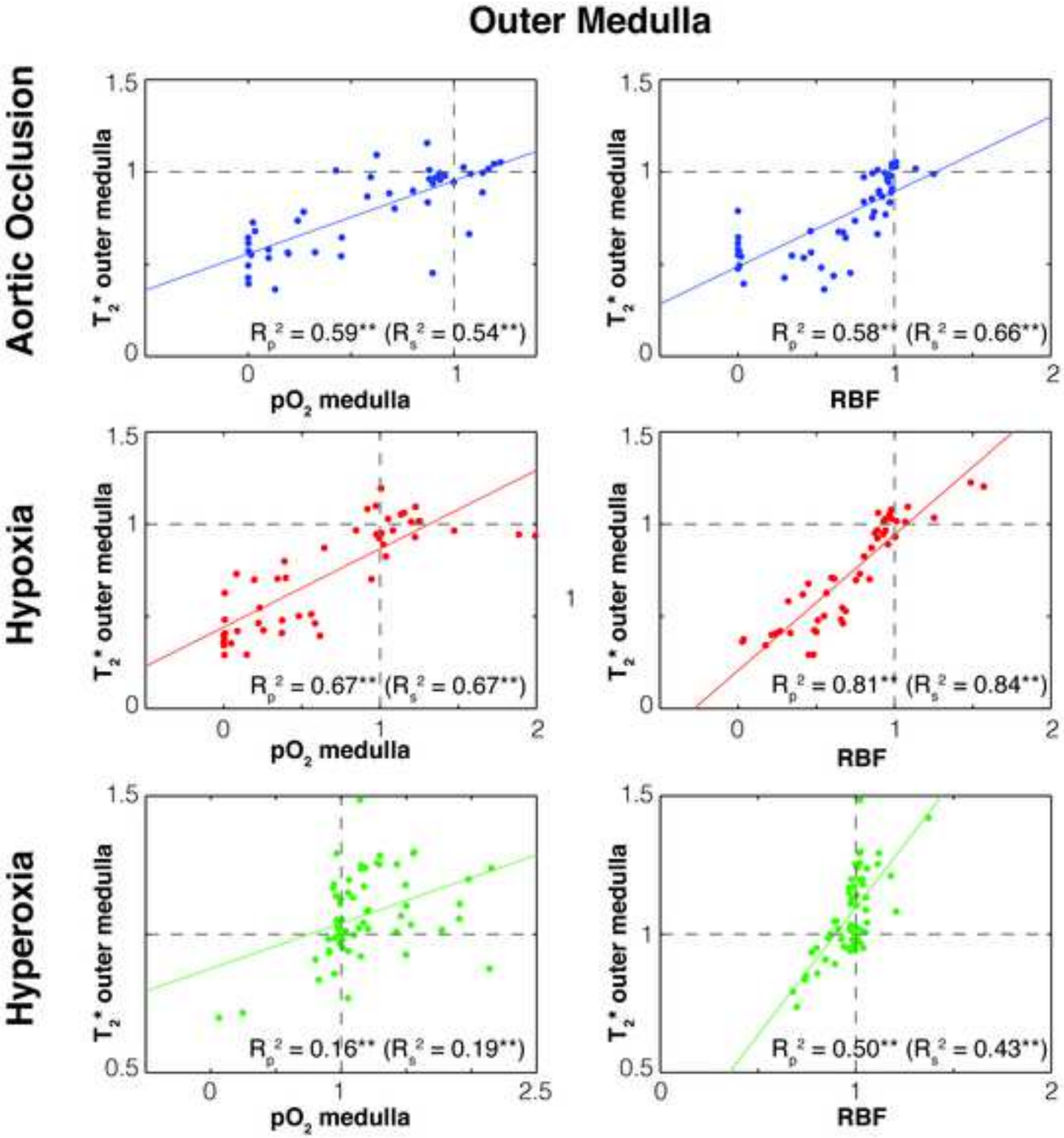
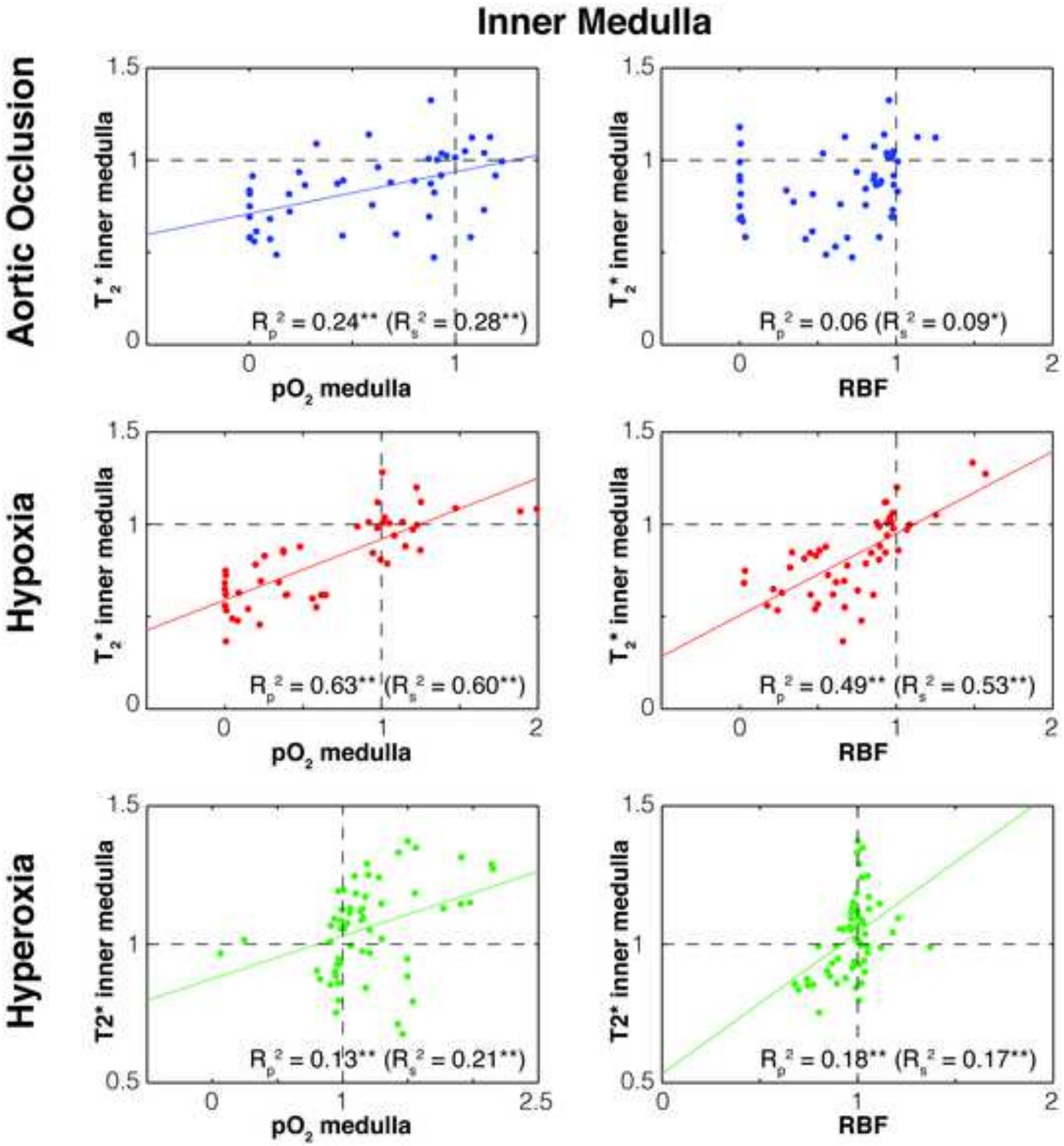
Figure 9 revised
Click here to download high resolution image